

Second, a positive curvature of the phase boundary occurs towards a high field. The positive curvature suggests that the transition field increases with temperature.

Field-induced superconductivity has been reported for paramagnetic $\text{Eu}_x\text{Sn}_{1-x}\text{Mo}_6\text{S}_8$ (ref. 10). This material is a superconductor with $T_c = 3.8\text{ K}$. As the magnetic field increases, the superconductivity is restored above 4 T and below 0.1 K, after it is destroyed at about 1 T. This phenomenon is well understood in terms of the Jaccarino–Peter compensation effect¹¹; the internal magnetic field created by the Eu moments through the exchange interaction is compensated by the external magnetic field. For λ -(BETS)₂FeCl₄, because an exchange interaction between the Fe moments and the conduction electrons is expected, the Jaccarino–Peter compensation effect may be a possible mechanism. However, this effect cannot explain how a very small amount of the magnetic field (at about 0.1 T) along the b^* axis destroys the superconducting state, because the paramagnetic Fe moments are aligned along the external field irrespective of the field direction. The surprisingly strong anisotropic superconducting transition for λ -(BETS)₂FeCl₄ suggests that the low dimensionality of the electronic system is closely related to the mechanism of the superconductivity.

For quasi-two-dimensional electronic systems such as λ -(BETS)₂FeCl₄, when a high magnetic field is applied exactly parallel to the conduction layers, the motion of the electrons is confined onto a single conduction layer. This is field-induced dimensional crossover from quasi-two-dimensional to two-dimensional. In this case, the orbital effect, one of the mechanisms destroying the superconductivity, is largely suppressed. However, if even a small amount of the magnetic field is perpendicular to the conduction layers, the electrons drift in the interlayer direction and the orbital effect is restored. This picture of dimensional crossover seems consistent with the experimental observation that very low magnetic fields along the b^* axis destroy superconductivity (Fig. 2a). On the basis of the dimensional crossover, various theoretical models predicting the existence of high-field superconducting phases have been proposed^{12–16}. However, all the theories tacitly assume that the superconductivity is stable at zero field.

The superconductivity of the iso-structural salt λ -(BETS)₂GaCl₄ ($T_c = 6\text{ K}$) survives in a magnetic field of up to 5 T that is perpendicular to the conduction layers¹⁷. This field is much larger than that for λ -(BETS)₂FeCl₄ (at about 0.1 T). We have carefully measured the resistance for λ -(BETS)₂GaCl₄ under fields exactly parallel to the conducting layers, but superconductivity was not restored at fields up to 20 T after the superconductivity was destroyed at around 13 T. The completely different phase diagrams of λ -(BETS)₂GaCl₄ and λ -(BETS)₂FeCl₄ suggest that the interaction between the Fe moments and the conduction electrons, as well as the low dimensionality of the electronic system, strongly affects the emergence of the superconductivity. It seems likely that the pairing interaction between the π electrons on the BETS molecules arises from the magnetic fluctuation through the paramagnetic Fe moments. □

Received 6 December 2000; accepted 14 February 2001.

- Chandrasekhar, B. S. A note on the maximum critical field of high-field superconductors. *Appl. Phys. Lett.* **1**, 7–8 (1962).
- Clogston, A. M. Upper limit for the critical field in hard superconductors. *Phys. Rev. Lett.* **15**, 266–267 (1962).
- Tinkham, M. *Introduction to Superconductivity* (McGraw-Hill, New York, 1975).
- Klemm, R. A., Luther, A. & Beasley, M. R. Theory of the upper critical field in layered superconductors. *Phys. Rev. B* **12**, 877–891 (1975).
- Brossard, L. *et al.* Interplay between chains of $S = 5/2$ localised spins and two-dimensional sheets of organic donors in the synthetically built magnetic multilayer λ -(BETS)₂FeCl₄. *Eur. Phys. J. B* **1**, 439–452 (1998).
- Kobayashi, H. *et al.* New BETS conductors with magnetic anions (BETS=bis(ethylenedithio)tetra-selenafulvalene). *J. Am. Chem. Soc.* **118**, 368–377 (1996).
- Kobayashi, H. *et al.* Electric and magnetic properties and phase diagram of a series of organic superconductors λ -(BETS)₂GaX₂Y₁₋₂ [X, Y=F, Cl, Br; $0 < z < 2$]. *Phys. Rev. B* **56**, R8526–R8529 (1997).

- Akutsu, H. *et al.* Highly correlated organic conductor with magnetic anions exhibiting a π -d coupled metal-insulator transition, λ -(BETS)₂FeBr₂Cl_{1-x}. *J. Am. Chem. Soc.* **119**, 12681–12682 (1997).
- Brooks, J. S., Naughton, M. J., Ma, Y. P., Chaikin, P. M. & Chamberlin, R. V. Small sample magnetometers for simultaneous magnetic and resistive measurements at low temperatures and high magnetic fields. *Rev. Sci. Instrum.* **58**, 117–121 (1987).
- Meul, H. W. *et al.* Observation of magnetic-field-induced superconductivity. *Phys. Rev. Lett.* **53**, 497–500 (1984).
- Jaccarino, V. & Peter, M. Ultra-high-field superconductivity. *Phys. Rev. Lett.* **9**, 290–292 (1962).
- Lebed, A. G. Reversible nature of the orbital mechanism for the suppression of superconductivity. *JETP Lett* **44**, 114–117 (1986).
- Dupuis, N., Montambaux, G. & Sa de Melo, C. A. R. Quasi-one-dimensional superconductors in strong magnetic field. *Phys. Rev. Lett.* **70**, 2613–2616 (1993).
- Miyazaki, M., Kishigi, K. & Hasegawa, Y. Superconductivity of quasi-one- and quasi-two-dimensional tight binding electrons in a magnetic field. *J. Phys. Soc. Jpn* **67**, 2618–2621 (1998).
- Shimahara, H. Coexistence of singlet and triplet attractive channels in the pairing interactions mediated by antiferromagnetic fluctuations. *J. Phys. Soc. Jpn* **69**, 1966–1969 (2000).
- Sa de Melo, C. A. R. Paramagnetism and reentrant behaviour in quasi-one-dimensional superconductors at high magnetic fields. *Physica C* **260**, 224–230 (1996).
- Tanatar, M. A. *et al.* Anisotropy of the upper critical field of the organic conductor λ -(BETS)₂GaCl₄. *J. Supercond.* **12**, 511–514 (1999).

Correspondence and requests for materials should be addressed to S.U. (e-mail: uji@nrim.go.jp).

Solid acids as fuel cell electrolytes

Sossina M. Haile, Dane A. Boysen, Calum R. I. Chisholm & Ryan B. Merle

Materials Science, California Institute of Technology, Pasadena, California 91125, USA

Fuel cells are attractive alternatives to combustion engines for electrical power generation because of their very high efficiencies and low pollution levels. Polymer electrolyte membrane fuel cells are generally considered to be the most viable approach for mobile applications. However, these membranes require humid operating conditions, which limit the temperature of operation to less than 100 °C; they are also permeable to methanol and hydrogen, which lowers fuel efficiency. Solid, inorganic, acid compounds (or simply, solid acids) such as CsHSO₄ and Rb₃H(SeO₄)₂ have been widely studied because of their high proton conductivities and phase-transition behaviour. For fuel-cell applications they offer the advantages of anhydrous proton transport and high-temperature stability (up to 250 °C). Until now, however, solid acids have not been considered viable fuel-cell electrolyte alternatives owing to their solubility in water and extreme ductility at raised temperatures (above approximately 125 °C). Here we show that a cell made of a CsHSO₄ electrolyte membrane (about 1.5 mm thick) operating at 150–160 °C in a H₂/O₂ configuration exhibits promising electrochemical performances: open circuit voltages of 1.11 V and current densities of 44 mA cm⁻² at short circuit. Moreover, the solid-acid properties were not affected by exposure to humid atmospheres. Although these initial results show promise for applications, the use of solid acids in fuel cells will require the development of fabrication techniques to reduce electrolyte thickness, and an assessment of possible sulphur reduction following prolonged exposure to hydrogen.

Solid acids are compounds such as KHSO₄ whose chemistry and properties lie between those of a normal acid (such as H₂SO₄) and a normal salt (such as K₂SO₄)¹. They are typically comprised of oxyanions—for example, SO₄ or SeO₄—that are linked together via O–H···O hydrogen bonds. Within this category the MHXO₄ and M₃H(XO₄)₂ compounds, where M = Cs, NH₄, Rb, and X = S or Se, are known to undergo a “superprotonic” phase transition^{2–9}. On passing through the transition the conductivity jumps by several orders of magnitude to a value of 10⁻³ to 10⁻² Ω⁻¹ cm⁻¹, and the

materials often become quite ductile. The transition temperatures typically lie between 50 and 150 °C, and the activation energy for transport in the high-temperature phase is 0.3 to 0.45 eV (Fig. 1). A key feature of the proton transport process is that, unlike polymeric systems, it does not require humid atmospheres.

Although superprotonic solid acids have excellent proton transport properties, they have not been considered for applications, not only because of their water solubility and unusual mechanical properties, but also because they simply have not come to the attention of the fuel-cell community. In this work, we have selected the solid acid CsHSO₄ for 'proof of principle' investigations in fuel-cell applications. This particular acid has been chosen because it is relatively well characterized and its superprotonic phase has a reasonably wide temperature range of stability, from the transition at 141 °C to decomposition/melting at approximately 200–230 °C (refs 5, 6). Membrane electrode assemblies (MEAs) were prepared as follows. A layer of the solid acid, synthesized from an aqueous solution of Cs₂CO₃ and H₂SO₄, was sandwiched between two electrocatalysis layers comprised of CsHSO₄, Pt black, carbon black and a volatile organic in a mass ratio of 6:10:1:1 (approximate volume ratio of 4:1:2:2). These layers were, in turn, placed between two sheets of porous, graphite, current collectors. The entire assembly was uniaxially pressed at 490 MPa, to yield a dense electrolyte membrane (1–1.5 mm in thickness) with good mechanical contact to the electrocatalyst layers. Fuel-cell polarization curves were collected at slightly raised temperatures from MEAs placed in a standard graphite test station. Upon heating to the measurement temperature, the organic phase in the electrode evaporated, leaving behind a porous electrode structure.

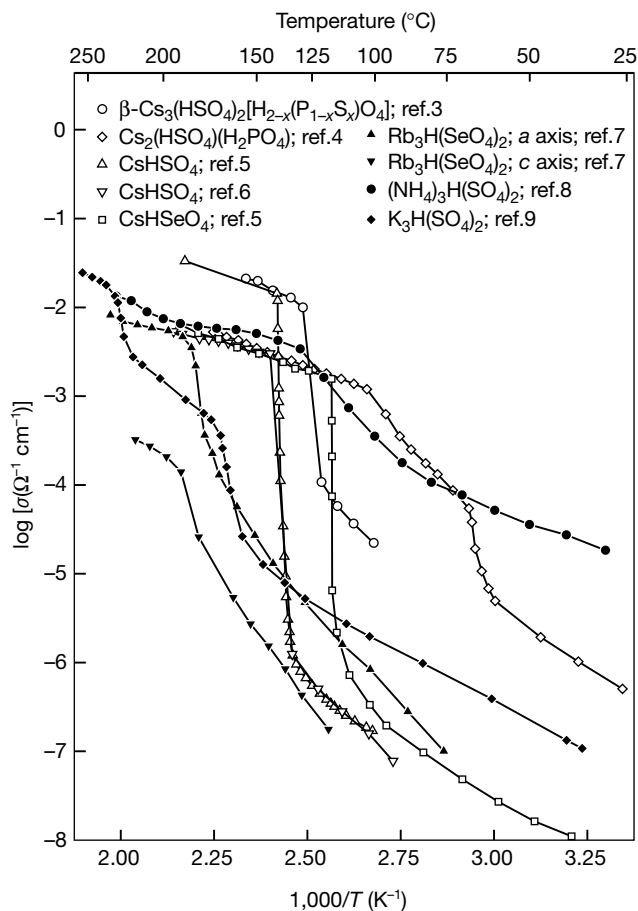


Figure 1 The conductivities of selected solid acids, shown in Arrhenius form. Sources as indicated on the figure.

The current densities of such a single-cell fuel cell, exposed to H₂O-saturated H₂ at the anode and H₂O-saturated O₂ at the cathode and held at 160 °C, are presented in Fig. 2. The platinum content or 'loading' was 18 mg cm⁻² and the membrane thickness 1.37 mm. The solid curve reflects the initial measurement and the dotted curve shows the measurement after 18 h of exposure to humid air. The anode and cathode gases were humidified during fuel-cell operation only in order to establish explicitly the open-circuit potential. Similar results were obtained for operation with dry gases. It is immediately apparent that despite the water solubility of CsHSO₄ and its ability to undergo extensive plastic deformation at high temperatures, stable fuel-cell performance is possible. The slight drop in performance with time is probably due to degradation at the anode as a result of interactions with H₂, as described below, and not a result of interactions with H₂O or any lack of dimensional integrity.

The open-circuit potential of the cell of Fig. 2 is 1.11 V. This compares favourably with the theoretical value of 1.22 V, expected for the conditions $T = 160\text{ °C}$, and the partial pressures $p_{\text{O}_2} \approx 1\text{ atm}$, $p_{\text{H}_2} \approx 1\text{ atm}$, and $p_{\text{H}_2\text{O}} = 3.13 \times 10^{-2}\text{ atm}$ (ref. 10). The difference between the measured and theoretical open circuit voltages (OCV) is probably due to gas permeability through residual pores within the polycrystalline electrolyte, or to slow gas leaks through the experimental apparatus. Nevertheless, the OCV obtained here is significantly higher than that typically observed in polymer-based

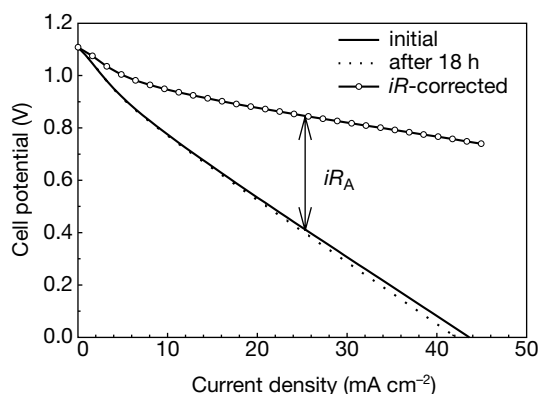


Figure 2 Cell voltage versus current density (polarization curve) for a CsHSO₄ fuel cell. It was operated at 160 °C under moist H₂ and moist O₂ at the anode and cathode respectively (total pressure of 1 atm). Platinum loading of 18 mg cm⁻². Solid line, initial measurement; dotted line, measurement after 18 h of exposure to humidified air at both electrodes; dashed-dotted line, *iR*-corrected result for initial measurement.

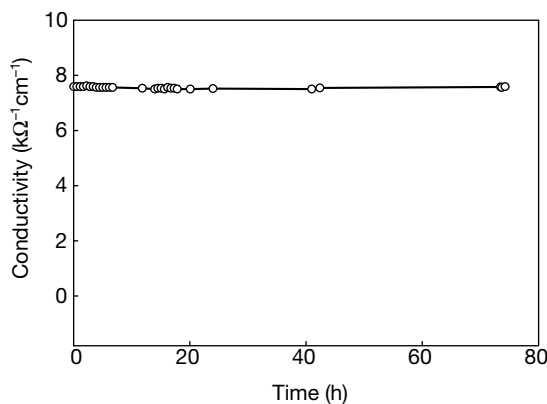


Figure 3 Conductivity of CsHSO₄ as a function of time at 146 °C and under humidified air. $p_{\text{H}_2\text{O}} = 3.13 \times 10^{-2}\text{ atm}$.

fuel cells: 0.9–1.0 V (ref. 11). The humidification requirements of the polymer, as well as its inherent permeability to O₂ and H₂ by molecular dissolution and transport, act to lower the maximum OCV achievable. In the case of the solid acid, we believe that improved processing will result in OCV values as high as the theoretical ones, as has been reported, for example, for KH₂PO₄ (ref. 12) and routinely for solid-oxide fuel cells¹³. Fuel-cell experiments in which dry gases were used yielded slightly higher OCVs up to 1.25 V, as we expected.

The drop in fuel-cell voltage with increasing current density (Fig. 2) has many causes¹¹; the primary of these, for a relatively thick electrolyte as was used in this experiment, is the resistance of the membrane. This term is given by iR_A , where i is the current density, and R_A is the area specific resistance, or t/σ , where t is the electrolyte thickness and σ is the conductivity. Thus, one expects a linear drop in voltage as a function of current density, the magnitude of which depends only on the properties and geometry of the electrolyte. The characteristics of the superprotonic phase transition of CsHSO₄ are well-established, but the reported conductivity at 160 °C varies from $3.70 \times 10^{-3} \Omega^{-1} \text{cm}^{-1}$ (ref. 6) to $2.08 \times 10^{-3} \Omega^{-1} \text{cm}^{-1}$ (ref. 5). Measurements in our laboratory under H₂O-saturated air indicate a conductivity of about $8 \times 10^{-3} \Omega^{-1} \text{cm}^{-1}$. Using this latter value and the electrolyte thickness of 1.37 mm, the expected slope in Fig. 2 is $-17.1 \Omega \text{cm}^2$, significantly smaller than the measured value of $-22.7 \Omega \text{cm}^2$. Additional resistance effects are probably due to slow charge transfer through the electrodes (also rather thick) and various contact resistances. The dashed-dotted curve in Fig. 2 ($E_{\text{meas}} + iR_A$) shows the magnitude of the losses due to all non-electrolyte factors. The electrode resistance was fairly insensitive to the Pt loading over the range examined, 3.8 mg cm⁻² to 38 mg cm⁻² (see Supplementary Information), which suggests that the electrode performance is not limited by the catalyst content, but rather by the electrode microstructure. Although these preliminary results demonstrate that the lower limit has not been reached, improved fabrication techniques will be necessary to further reduce Pt loadings.

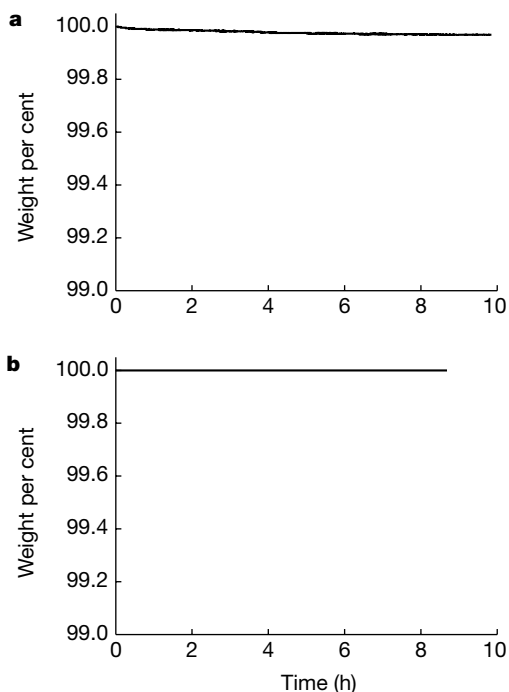
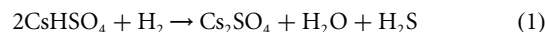


Figure 4 Weight as a function of time of CsHSO₄ at 160 °C. **a**, Under flowing H₂; **b**, under flowing O₂.

In this work we used rather thick membranes to obtain impermeable MEAs and stable OCVs. In order to achieve an area-specific resistivity that is directly comparable to that of Nafion membranes (typically 0.025 to 0.0875 Ωcm^2 at 90 °C and under highly humidified atmospheres for membranes 50–175 μm in thickness¹¹) a dense CsHSO₄ membrane with a thickness of the order of 2–20 μm would be necessary. Such films may not be immediately achievable, but routine fabrication of solid-oxide electrolytes with comparable dimensions¹⁴ renders this target quite realistic.

In order to assess the stability of CsHSO₄ under fuel-cell conditions, several longevity experiments were carried out. To examine the impact of humid conditions, its conductivity was measured at 146 °C under H₂O-saturated air by impedance spectroscopy. For this experiment, electrodes were attached in a manner identical to that used for MEA fabrication. To examine the impact of reducing and oxidizing atmospheres, thermal gravimetric analysis was carried out under flowing H₂ and flowing O₂, respectively. The results of the conductivity measurements are presented in Fig. 3, and the results of the thermal analyses are displayed in Fig. 4. The data in Fig. 3 demonstrate that the conductivity of CsHSO₄ is absolutely stable over tens of hours in humid atmospheres. Similarly, the results in Fig. 4 reveal that the solid acid is completely stable under oxidizing conditions, as expected. Under reducing conditions, however, the material has lost 0.03 wt% over 10 h. This weight loss is probably due to gradual sulphur reduction according to reaction (1), which, in turn, may be responsible for the slight loss in fuel-cell performance (Fig. 2) via the production of the catalyst poison, H₂S.



The potential for sulphur reduction in solid-acid sulphates indicates that ultimately alternative oxyanion systems such as phosphates (for example, CsH₂PO₄; ref. 15) and complex heteropolyacids (for example, H₃PW₁₂O₄₀·nH₂O; ref. 16), which are not susceptible to reduction, may be the solid acid of choice for fuel-cell applications.

The results shown in Figs 2–4 demonstrate that inorganic, water-soluble solid acids can be used successfully in H₂/O₂ fuel cells, and that MEAs fabricated from these materials yield higher OCVs than those obtained from polymer-electrolyte fuel cells. Higher OCVs, in turn, may lead to better overall system efficiencies. Further advantages that may ultimately result from such inorganic, non-hydrated electrolytes are: greater tolerance of the catalysts to CO due to slightly raised temperatures of operation; reduction in system complexity by elimination of costly temperature and humidity monitoring and control hardware; and applicability in direct (vapour) methanol fuel cells without methanol cross-over losses¹⁷. Several challenges remain before these advantages can be realized, including: (1) processing of thin, impermeable solid-acid membranes, (2) enhancement of electrode performance, and (3) system design to protect the electrolyte from liquid water during both intentional and inadvertent fuel-cell shut-off. Moreover, phosphate or other oxyanion-based superprotonic conductors may be preferable for long-term stability over those based on sulphates or selenates. □

Received 19 September 2000; accepted 22 February 2001.

- Wells, A. F. *Structural Inorganic Chemistry* 3rd edn, 300–303 (Clarendon, Oxford, 1984).
- Haile, S. M., Lentz, G., Kreuer, K.-D. & Maier, J. Superprotonic conductivity in Cs₃(HSO₄)₂(H₂PO₄). *Solid State Ion.* **77**, 128–134 (1995).
- Haile, S. M., Calkins, P. M. & Boysen, D. Superprotonic conductivity in β -Cs₃(HSO₄)₂(H₂(P(S)O₄)). *Solid State Ion.* **97**, 145–151 (1997).
- Chisholm, C. R. I. & Haile, S. M. Superprotonic behavior of CsHSO₄–CsH₂PO₄ system. *Solid State Ion.* **136–137**, 229–241 (2000).
- Baranov, A. I., Shuvalov, L. A. & Shchagina, N. M. Superior conductivity and phase transitions in CsHSO₄ and CsHSeO₄ crystals. *JETP Lett.* **36**, 459–462 (1982).
- Norby, T., Friesel, M. & Mellander, B. E. Proton and deuteron conductivity in CsHSO₄ and CsDSO₄ by in situ isotopic exchange. *Solid State Ion.* **77**, 105–110 (1995).
- Pawłowski, A., Pawłaczyk, Cz. & Hilzler, B. Electric conductivity in crystal group Me₃H(SeO₄)₂ (Me: NH₄⁺, Rb⁺, Cs⁺). *Solid State Ion.* **44**, 17–19 (1990).

8. Ramasastry, C. & Ramaiah, A. S. Electrical conduction in $\text{Na}_3\text{H}(\text{SO}_4)_2$ crystals. *J. Mater. Sci. Lett.* **16**, 2011–2016 (1981).
9. Chisholm, C. R. I., Merinov, B. V. & Haile, S. M. High temperature phase transitions in $\text{K}_3\text{H}(\text{SO}_4)_2$. *Solid State Ion.* (in the press).
10. Gaskell, D. R. *Introduction to Metallurgical Thermodynamics* 2nd edn, 574 & 586 (McGraw-Hill, Washington DC, 1981).
11. Srinivasan, S., Velev, O. A., Parthasarathy, A., Manko, D. J. & Appleby, A. J. High energy efficiency and high power density proton exchange membrane fuel cells—electrode kinetics and mass transport. *J. Power Sources* **36**, 299–320 (1991).
12. Croce, F. & Cigna, G. Determination of the protonic transference number for KH_2PO_4 by electro-motive force measurements. *Solid State Ion.* **6**, 201–202 (1982).
13. Minh, N. Q. Ceramic fuel cells. *J. Am. Ceram. Soc.* **76**, 563–588 (1993).
14. Minh, N. Q. & Horne, C. R. in *Proc. 14th Riso Int. Symp. on Materials Science: High Temperature Electrochemical Behaviour of Fast Ion and Mixed Conductors* (eds Poulsen, F. W., Bentzen, J. J., Jacobsen, T., Skou, E. & Østergård, M. J. L.) 337–341 (Riso National Laboratory, Roskilde, 1993).
15. Baranov, A. I., Khiznichenko, V. P., Sandler, V. A. & Shuvalov, L. A. Frequency dielectric dispersion in the ferroelectric and superionic phases of CsH_2PO_4 . *Ferroelectrics* **81**, 183–186 (1988).
16. Slade, R. C. T. & Omana, M. J. Protonic conductivity of 12-tungstophosphoric acid (TPA, $\text{H}_3\text{PW}_{12}\text{O}_{40}$) at elevated temperatures. *Solid State Ion.* **58**, 195–199 (1992).
17. Haile, S. M., Narayanan, S. R., Chisholm, C. & Boysen, D. Proton conducting membrane using a solid acid. US patent 09/439,377 (15 Nov. 2000).

Supplementary information is available on Nature's World-Wide Web site (<http://www.nature.com>) or as paper copy from the London editorial office of Nature.

Acknowledgements

We thank J. Snyder for assistance with computer automation of the fuel cell test station and S. R. Narayanan for technical discussions. Financial support has been provided by the California Institute of Technology through the Yuen Grubstake entrepreneurial fund.

Correspondence and requests for materials should be addressed to S.M.H. (e-mail: smhaile@caltech.edu).

Self-assembly of mesoscopically ordered chromatic polydiacetylene/silica nanocomposites

Yunfeng Lu^{*†‡§}, Yi Yang[†], Alan Sellinger^{‡§}, Mengcheng Lu[†], Jinman Huang[†], Hongyou Fan[‡], Raid Haddad[†], Gabriel Lopez[†], Alan R. Burns[‡], Darryl Y. Sasaki[‡], John Shelnutt[‡] & C. Jeffrey Brinker^{†‡§}

[†]The University of New Mexico Center for Micro-Engineered Materials and Department of Chemical and Nuclear Engineering, Albuquerque, New Mexico 87131, USA

[‡]Sandia National Laboratories, Advanced Materials Laboratory, 1001 University Blvd SE, Albuquerque, New Mexico 87106, USA

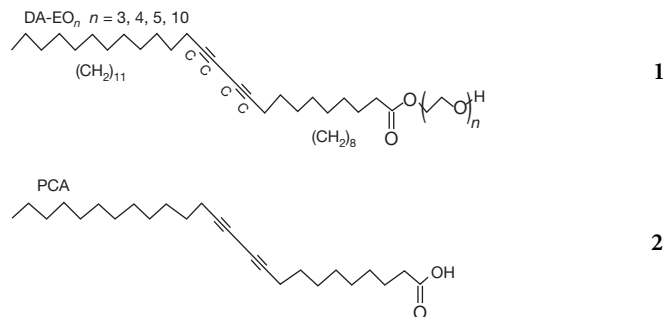
[§]These authors contributed equally to this work.

Nature abounds with intricate composite architectures composed of hard and soft materials synergistically intertwined to provide both useful functionality and mechanical integrity. Recent synthetic efforts to mimic such natural designs have focused on nanocomposites^{1–5}, prepared mainly by slow procedures like monomer or polymer infiltration of inorganic nanostructures^{6,7} or sequential deposition^{8,9}. Here we report the self-assembly of conjugated polymer/silica nanocomposite films with hexagonal, cubic or lamellar mesoscopic order using polymerizable amphiphilic diacetylene molecules as both structure-directing agents and monomers. The self-assembly procedure is rapid and incorporates the organic monomers uniformly within a highly

ordered, inorganic environment. Polymerization results in polydiacetylene/silica nanocomposites that are optically transparent and mechanically robust. Compared to ordered diacetylene-containing films prepared as Langmuir monolayers¹⁰ or by Langmuir–Blodgett deposition¹⁰, the nanostructured inorganic host alters the diacetylene polymerization behaviour, and the resulting nanocomposite exhibits unusual chromatic changes in response to thermal, mechanical and chemical stimuli. The inorganic framework serves to protect, stabilize, and orient the polymer, and to mediate its function. The nanocomposite architecture also provides sufficient mechanical integrity to enable integration into devices and microsystems.

Owing to extended π -electron delocalization along their backbones, conjugated organic polymers exhibit electronic and optical properties of interest for applications ranging from light-emitting diodes to biomolecular sensors¹¹. For example, in blue-coloured polydiacetylene, the optical absorption blue-shifts dramatically when stress is applied to the backbone through the pendant side chains, and this thermally, mechanically, or chemically induced chromatic (blue \rightarrow red) response has been explored as a colorimetric transduction scheme in a variety of chemically and physically based sensor designs^{12,13}. Further improvements of the electronic and optical performance of conjugated polymer devices may require polymer incorporation in nano-engineered architectures¹⁴ that could provide alignment, control charge and energy transfer, mediate conformational changes and prevent oxidation. Recently control of energy transfer was demonstrated in a poly[2-methoxy-5-(2'-ethyl-hexyloxy)-1,4-phenylene vinylene] (MEH-PPV)/silica nanocomposite⁷. However, this nanocomposite, prepared by MEH-PPV infiltration of a pre-formed, oriented, hexagonal, silica mesophase, was heterogeneous, exhibiting two distinct conjugated polymer environments, that is, polymers inside and outside the hexagonally arranged pore channels of the silica particles. In general, because polymer infiltration into a pre-formed porous nanostructure depends on the partitioning of the polymer from the solvent, we expect it to be difficult to control polymer concentration, orientation and uniformity in the corresponding nanocomposite. Further, when the nanostructure pore size is less than the radius of gyration of the solvated polymer, infiltration proceeds by a worm-like motion referred to as reptation, requiring long processing times at elevated temperatures⁷.

We use a series of oligoethylene glycol functionalized diacetylenic (DA-EO_n) surfactants (structure 1, with $n = 3, 4, 5, 10$), prepared by coupling ethylene glycols with the acid chloride of PCA (structure 2)



both as amphiphiles to direct the self-assembly of thin film silica mesophases¹⁵ and as monomeric precursors of the conjugated polymer, polydiacetylene (PDA). Beginning with a homogeneous solution of silicic acid and surfactant prepared in a tetrahydrofuran (THF)/water solvent with initial surfactant concentration c_0 much less than the critical surfactant micelle concentration CMC, we use evaporative dip-coating, spin-coating, or casting procedures to prepare thin films on silicon (100) or fused silica substrates (Fig. 1). During deposition, preferential evaporation of THF

[§] Present address: Tulane University Chemical Engineering Department, New Orleans, Louisiana 70118, USA (Y.L.); Canon Research and Development Center Americas, San Jose, California 95134, USA (A.S.).